The Astrophysical Journal, 642:371–381, 2006 May 1

QUANTIFYING THE LUMINOSITY EVOLUTION IN GAMMA-RAY BURSTS

Dan Kocevski[1] and Edison Liang[2]

Received 2005 July 8; accepted 2005 December 12

ABSTRACT

We estimate the luminosity evolution and formation rate for more than 900 GRBs by using redshift and luminosity data calculated by Band, Norris, & Bonnell via the lag-luminosity correlation. By applying maximum likelihood techniques, we are able to infer the true distribution of the parent GRB population's luminosity function and density distributions in a way that accounts for detector selection effects. We find that after accounting for data truncation, there still exists a significant correlation between the average luminosity and redshift, indicating that distant GRBs are on average more luminous than nearby counterparts. This is consistent with previous studies showing strong source evolution and also recent observations of underluminous nearby GRBs. We find no evidence for beaming angle evolution in the current sample of GRBs with known redshift, suggesting that this increase in luminosity cannot be due to an evolution of the collimation of gamma-ray emission. The resulting luminosity function is well fit with a single power law of index $L'^{-1.5}$, which is intermediate between the values predicted by the power-law and Gaussian structured jet models. We also find that the GRB comoving rate density rises steeply, with a broad peak between $1 = z = 2$ followed by a steady decline above $z > 3$. This rate density qualitatively matches the current estimates of the cosmic star formation rate, favoring a short-lived massive star progenitor model or a binary model with a short delay between the formation of the compact object and the eventual merger.

Subject headings: gamma rays: bursts — gamma rays: theory

Online material: color figure

1. INTRODUCTION

There are currently roughly three dozen gamma-ray burst events (GRBs) for which we have independently measured redshifts. Most of these redshift determinations come from either identification of absorption lines in the afterglow spectra, attributed to the gas in the host galaxy, or from observations of emission lines from the host galaxy. The combination of these techniques has resulted in a small but growing GRB sample with redshifts ranging from 0.0085 to 4.5 and a distribution peaking around $z \sim 1$. From this small sample, it is already abundantly clear that the isotropic equivalent energy $E_{\rm iso}$ released in the prompt GRB phase is not a standard candle. The total radiated energy taken at face value (i.e., when not correcting for a beaming factor $d\Omega$) clearly spans several orders of magnitude, ranging from 10^{47} for the closest event, GRB 980425 at $z = 0.0085$ (Kulkarni et al. 1998), to 10^{54} for GRB 990123 at $z = 1.6004$ (Kulkarni et al. 1998). Recently Sazonov et al. (2004) and Soderberg (2004) have reported on gamma-ray observations of a nearby underluminous GRB occurring at redshift of $z = 0.106$. These new findings have added to the speculation that there is either a substantial underluminous population of GRBs that cannot be seen at large distances and/or that nearby events ($z < 0.15$) are underluminous compared to distant counterparts, pointing to the evolution of the average energy emitted by a GRB with time.

A measure to the extend to which luminosity evolution exists in the GRB population, along with their true luminosity function and density distribution, may yield important clues regarding the nature of gamma-ray bursts and how they're progenitors have evolved with time. Although the physics of the underlying GRB engine is hidden from direct observation and is yet uncertain, the total GRB energy budget is most likely linked to the mass and/or rotational energy of the GRB progenitor. Understanding of how this energy budget has changed with time may offer constraints on progenitor properties and may ultimately point to the physics leading to their explosions. Since GRB progenitors are most likely linked to compact objects (supermassive rotating star, black hole, or neutron star mergers) understanding how the GRB luminosity function evolves with time may give insight to the host environment in the early universe, namely, the star formation rate (SFR) or initial stellar mass functions at high redshifts.

Any attempt at quantifying the evolution of intrinsic source properties of parent populations must account for Malquist type biases. Detection thresholds prevent events below a certain flux from being observed, resulting in the detection of only bright objects at large distances. Combined with the fact that bright events are typically rare, it is very easy in astronomy to incorrectly conclude that the distant universe is filled with extremely bright rare objects. Any attempt at measuring the correlation between luminosity and redshift without properly accounting for selection effects will grossly overestimate the correlation strength between the two variables. Flux-limited samples are a classic problem in astronomy, which manifested prominently in early quasar studies. Fortunately, straightforward methods have been devised to account for such effects based on maximum likelihood techniques. These methods allow for the correct estimation of the correlation strength between a truncated data set, as well as providing an estimate on the underlying parent population. The "catch" involved in such techniques is that the overall normalization of the resulting parent distributions cannot be determined, although their functional forms are constructed in such a way as to account for the data truncations.

These techniques also have the limitation of requiring large sample sizes and, more importantly, an extremely good understanding of the survey's detection thresholds (i.e., the flux cutoff for magnitude limited samples). The use of the current sample of GRBs with known redshift is limited by both of these restrictions. The

[1] Physics Department, 366 Le Conte Hall, University of California, Berkeley, CA 94709; kocevski@berkeley.edu.

[2] Department of Physics and Astronomy, Rice University, 6100 Main Street, Houston, TX 77005; liang@spacibm.rice.edu.

current size of a little over two dozen bursts does not lend itself well to producing statistically robust results, especially in the high- and low-redshift regimes for which only a handful of events have been detected. Furthermore, the sample is an accumulation of observations from several different spacecraft, all of varying detector thresholds. It would seem that these limitations could only be overcome by the accumulation of a larger data set with consistent detector thresholds, which is expected to come from the *Swift* spacecraft and the upcoming *Gamma-Ray Large Area Space Telescope* (*GLAST*) mission.

Fortunately, several authors have announced empirical Cepheid-like correlations linking intrinsic burst properties, such as luminosity (Norris et al. 2000) and the total radiated energy (Amati et al. 2002; Ghirlanda et al. 2004) to other GRB observable. These correlations may allow for the determination of burst redshifts directly from the gamma-ray data, which has the advantage of being relatively insensitive to extinction and observable at far greater distances than afterglow line measurements. The first of these correlations was reported by Norris et al. (2000). Using six BATSE-detected bursts with known redshift, they found an anticorrelation between the *source* frame lag between the 25–50 keV and 100–300 keV emission and the absolute luminosity of the GRB. More recently, (Ghirlanda et al. 2004) reported an empirical correlation between the collimation correction total energy E_γ radiated by the burst and the rest-frame energy at which most of the prompt radiation is emitted $E_{\rm pk}$. Using these relationships, it is now possible to estimate "pseudo"-redshifts for a much larger number of GRBs detected by the BATSE instrument, which previously lacked any information as to their distance. More importantly, the BATSE detector threshold is relatively well understood for the entire sample, making the resulting pseudo-redshift data excellent for statistical analysis.

In this paper, we examine the issue of luminosity and density evolution by using a sample of over 900 BATSE GRBs for which the luminosity and redshift where recently estimated by Band et al. (2004) through the use of the lag-luminosity correlation. We limit our analysis to the lag-luminosity correlation primarily due to the lack of jet opening angle θ_j information that is required for the use of the E_γ-$E_{\rm pk}$ relation. This relationship requires knowledge of θ_j in order to determine the collimation factor, which is only known for bursts with measured jet break times and hence cannot be used with the BATSE sample in consideration for this paper. To this sample, we apply statistical techniques developed by Lynden-Bell (1971) and Efron & Petrosian (1992) and first applied to GRB analysis by Lloyd-Ronning et al. (2002) to measure the underlying luminosity and density distribution in a way that properly accounts for the detection thresholds of the BATSE instrument. We find a strong (11.63 σ) correlation between luminosity and redshift, which can be parameterized as $L(z) = (1+z)^{1.7\pm0.3}$. The resulting cumulative luminosity function $N(L')$ is well fit by double power law separated by a break energy of about 10^{52} ergs s^{-1}, with the differential luminosity function dN/dL' exhibiting a power-law shape of $L^{-1.5}$ below this luminosity. We show that the GRB comoving rate density increases roughly as $\rho_\gamma(z) \propto (1+z)^{2.5}$ to a redshift of $z \approx 1$ followed by a flattening and eventual decline above $z > 3$. This rate density is in qualitative agreement with recent photometric estimates of the cosmic SFR, as would be expected from massive short-lived progenitors.

In § 2 we describe the data set that we use in our study. In § 3 we discuss the statistical methods applied to these data to estimate the GRB luminosity function and comoving rate density, as well as to test for any correlation between luminosity and redshift. In § 4 we present the resulting demographic distribution functions of this analysis, followed in § 5 by a discussion of the implications of the shape and evolution of the luminosity function and comoving rate density on various jet profile. We show that there is no evidence for beaming angle evolution in the current sample of GRBs with known redshift, suggesting that the variation of the observed luminosity with redshift cannot be due to an evolution of the collimation of gamma-ray emission. We conclude by examining how the similarity between the SFR and the GRB comoving rate density tentatively favors short-lived progenitor models.

2. DATA

For this analysis we use data for 1438 BATSE detected GRBs presented in Band et al. (2004, hereafter BNB04). This sample includes peak photon flux $f_{\rm pk}$ in the 50–300 keV band on a 256 ms timescale, the burst duration T_{90}, and measured lags and their uncertainties for each burst. From these lag measurements, the authors infer each burst's luminosity and redshift by using the lag-luminosity correlation, allowing also for an estimation of the intrinsic $E_{\rm pk}$ and $E_{\rm iso}$ for each burst. Of these 1438 bursts, 1218 have positive lags, making them suitable for this analysis. These data are shown in Figure 1 with an imposed flux cut set at 0.5 photons cm^{-2} s^{-1}, leaving a total of 985 bursts.

The lag measurements used in this sample were made using a cross-correlation analysis similar to that previously employed by Band et al. (1993) and Norris et al. (2000). The cross-correlation method has been widely used in X-ray and gamma-ray astronomy and is well suited for a timing analysis between two signals. In this application the normalized discrete cross-correlation function is given by

$$\mathrm{CCF}(\tau) = \sum_{i}^{N-1} \frac{f_i(t) g_i(t-t')}{\sigma_f \sigma_g}, \qquad (1)$$

where t' is commonly referred to as the lag between $f(t)$ and $g(t)$ and $\sigma_f = \langle f(t)^2 \rangle^{1/2}$. By maximizing the CCF function (i.e., by maximizing the area of the product of the two functions) as a function of t', an estimate of the temporal offset of the two signals can be made. If $g(t)$ leads $f(t)$ by t_0 [i.e., $f(t) = g(t+t_0)$], then the CCF curve peaks at $t' = t_0$.

In BNB04, the authors use 64 ms count data gathered by the BATSE Large Area Detectors (LADs), which provide discriminator rates with 64 ms resolution from 2.048 s before the burst to several minutes after the trigger (Fishman et al. 1994). The discriminator rates are gathered in four broad energy channels covering approximately 25–50, 50–100, 100–300, and 300 to about 1800 keV, allowing for excellent count statistics, since the photons are collected over a wide energy band. BNB04 measure the temporal offset or lag between channel 3 (100–300 keV) and channel 1 (25–50 keV) light curves to produce the CCF31 lags listed in their sample.

The shifting of the GRB spectra out of (or into) the observers frame, otherwise known as the *k*-correction, was accounted for in the analysis performed in BNB04. They perform spectral fits for most of the bursts in their sample, and for those that cannot yield a fit, a "Band" spectral model with average parameters is assumed for the spectra. The effects of time dilation and *k*-correction are then used to obtain the source frame lag and are also applied to the energy flux to obtain a bolometric luminosity.

As was the case in the original Norris et al. (2000) paper, the CCF method used in BNB04 can result in lag measurements that are less than the 64 ms time resolution of the BATSE instrument. In these cases, the associated errors of these values tend to

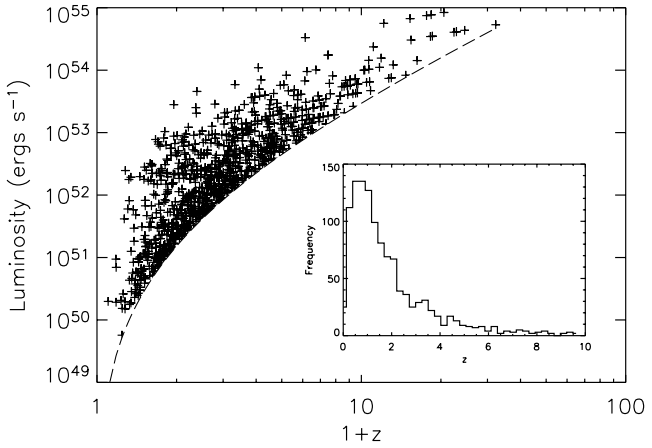

FIG. 1.—Luminosity and redshift data used in our analysis as deduced from the lag-luminosity correlation. The dashed line represents an imposed 0.5 photons cm^{-2} s^{-1}. . . , cut to the original 1438 bursts analyzed by BNB04, producing the sharp cutoff in the data. This leaves a total of 985 bursts with a median redshift of 1.64.

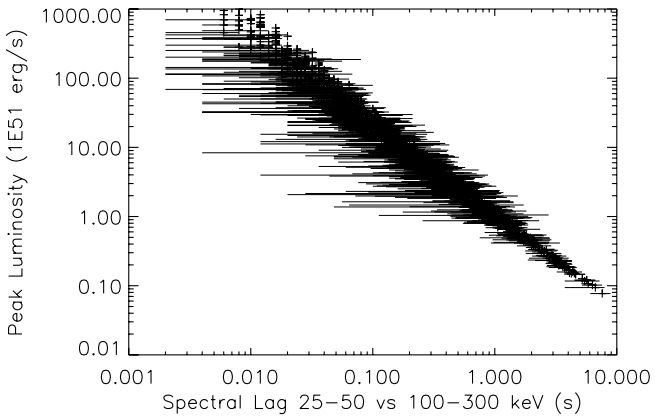

FIG. 2.—Plot of the lag-luminosity plane for the events under consideration. The errors in the lag and flux measurements are used to determine the uncertainty in the luminosity values, which in effect is used as a weight in the maximum likelihood technique that estimates the correlation strength between L and z.

be quite large, reducing the significance of their associated luminosity and redshift values. These errors are taken into consideration in the maximum likelihood techniques performed in our analysis. Therefore, bursts with extremely short lags (and hence high luminosities) are weighted accordingly. A plot of the lag-luminosity plane for the events under consideration, along with the errors in the lag measurements, is shown in Figure 2.

2.1. *Estimating Redshifts*

Using these lag measurements, BNB04 use the lag-luminosity correlation to estimate the luminosity of each event. This empirical correlations was reported by Norris et al. (2000), who used the CCF method to measure the lag between the BATSE channel 3 and channel 1 energy light curves for six GRBs with independently measured redshift. They concluded that there was an anticorrelation between the *source* delay in the low- and high-energy emission and the absolute luminosity of the GRB showing that high-luminosity events exhibited very small intrinsic (source frame) lag, whereas fainter bursts exhibited the largest time delay. This empirical correlation can be expressed as

$$L = 2.51 \times 10^{51} (\Delta t'/0.1)^{-1.15}, \tag{2}$$

where $\Delta t'$ is the source frame lag related to the observed lag $\Delta t'_{\rm obs}$ by a time dilation factor of $(1+z)^{-1}$. The fact that the lag-luminosity correlation relates two source frame quantities (i.e., luminosity and intrinsic lag) would make it seem that knowledge of the redshift is needed a priori. As it turns out, this is not the case. A simple numerical iteration routine can be used to solve for the redshift of a GRB that lacks any information as to its distance. This is done by first making an initial guess for z (say $z \sim 1$) to obtain the lag in the comoving frame $\Delta t' = \Delta t'_{\rm obs}/(1+z)$. This in turn gives us an initial value for the luminosity through the use of the lag-luminosity relation. This luminosity is then used in combination with the burst's energy flux to obtain a value for the luminosity distance D_L through the standard relation

$$D_L = \sqrt{\frac{L/d\Omega}{f_{256}}}, \tag{3}$$

where f_{256} is the peak flux in the 256 ms timescale and $d\Omega$ is the beaming factor. This distance is then compared to the D_L that can be calculated directly from the guessed redshift z by assuming standard cosmological parameters ($H_0 = 65$ km s^{-1}, $\Omega_m = 0.3$, and $\Omega_\Lambda = 0.7$) and using the expression:

$$D_L = (1+z)\frac{c}{H_0}\int_0^z \frac{dz}{\sqrt{\Omega_m (1+z)^3 + \Omega_\Lambda}}. \tag{4}$$

The value for z is then varied until the luminosity distances obtained from the two separate methods converge to within some predetermined precision.

We note that it has been suggested by Salmonson (2001) and Norris (2002) that the lag-luminosity relationship should be a broken power law in order to accommodate GRB 980425. This burst was associated with SN 1998bw, and when using the distance to the supernova, the GRB appears underluminous compared to the other bursts that fall on the lag-luminosity correlation. In their analysis, BNB04 note that this break has been suggested to fit a single point, which may or may not be associated with the SNe event, and hence decide to use a single power law of -1.15.

The physical origin of the lag-luminosity correlation is not immediately clear. Fundamentally, this observed lag is due to the evolution of the GRB spectra to lower energies, so a relationship between the rate of spectral decay and luminosity is expected (Kocevski & Liang 2003). This implies that the mechanisms resulting in the "cooling" of the GRB spectra is intimately related to the total energy budget of a GRB or its collimation factor. Other proposed theories attempt to explain the lag-luminosity correlation as being due to the effect of the viewing angle of the GRB jet (Kobayashi et al. 2002; Ioka & Nakamura 2001) and/or kinematic effects (Salmonson 2000). In any case, the use of this correlation is similar to methods used to calibrate Type Ia supernova luminosities based on the empirical correlation between their peak magnitude and rate of light-curve decay (Phillips et al. 1999). The lack of a clear physical interpretation of these correlations does not immediately preclude their use in determining, or refining, luminosity estimates.

3. ANALYSIS

The luminosity and redshift data calculated by BNB04 give us an enormous sample with which to investigate the evolution of the GRB luminosity function. As with any cosmological source, it is important and revealing to understand how the average

luminosity and density has evolved with cosmic time. Attempting to do so by simply measuring the correlation coefficient between the flux truncated luminosity and redshift data in the BNB04 sample without properly accounting for the detector selection effects would grossly overestimate the correlation strength. This is true whenever an estimate of correlation is made between two variables that suffer from data truncations, with the resulting correlation coefficient representing the truncation itself and not the underlying relation.

There have been several methods developed in astronomy to account for such selection effects, based largely on maximum likelihood techniques (see Petrosian 1992 for a review). In our analysis we use a nonparametric statistical technique originally proposed by Lynden-Bell (1971) for applications in flux-limited quasar studies. This so-called *C* method has been used successfully to reconstruct underlying parent distributions for quasars and GRBs samples by Maloney & Petrosian (1999) and Lloyd-Ronning et al. (2002), respectively. The parent luminosity and redshift distributions that the method estimates allows for the construction of a GRB luminosity function, a measure of the number of bursts per unit luminosity, and an estimate on the comoving rate density, a measure of the number of bursts per unit comoving volume and time.

The *C* method has two important limitations, or stipulations, to its use. First, the truncation limit below which no observations can be made must be well known. This is not a problem in our case, since the detector threshold of the BATSE instrument is well understood and BNB04 quantify the truncation limit of their sample. Second, the parent luminosity and redshift distributions can only be estimated in a bivariate manner if the two variables are uncorrelated. This is a limitation of all nonparametric techniques that rely on the assumption of stochastic independence. Therefore, it is necessary to first determine the degree of correlation between the two variables, in our case luminosity and $Z = 1 + z$, and then produce an uncorrelated data set through the transformation $L \rightarrow L' = L/g(z)$, where $g(z)$ parameterizes the luminosity evolution. Using this uncorrelated data set, it is then possible to apply the *C* method to estimate the underlying parent luminosity and redshift distributions. To estimate the degree of correlation we use a simple test of independence for truncated data put forth by Efron & Petrosian (1992), which is based in part on Lynden-Bell's *C* method. Below we describe the details of both Lynden-Bell's *C* method and the Efron & Petrosian independence test and how they are applied in our analysis.

3.1. *Test of Independence*

If the variables x and y in a data set are independent, then the rank R_i of x_i within that set should be distributed uniformly between 1 and N, with an expected mean $E = (1/2)(N + 1)$ and variance $V = (1/12)(N^2 - 1)$. It is common practice to normalize the rank R_i such that for independent variables R_i has a mean of 0 and a variance of 1 by defining the statistic $T_i = (R_i - E)/V$. A specialized version of the Kendell τ statistic can be constructed to produce a single parameter whose value directly rejects or accepts the hypothesis of independence. This quantity is commonly defined as

$$\tau = \frac{\Sigma_i (R_i - E)}{\sqrt{\Sigma_i V}}. \tag{5}$$

Based on this definition, a τ of 1 indicates a 1 σ correlation whereas a τ of 0 signifies a completely random data set. See Efron & Petrosian (1992) for a more detailed (and elucidating) proof of the applicability of normalized rank statistics.

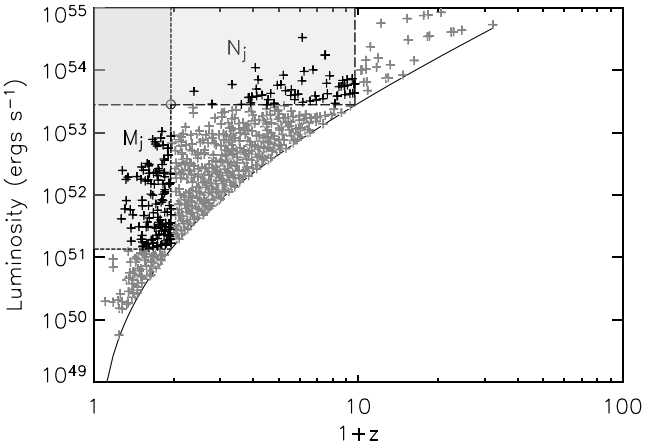

FIG. 3.—Representation of the associated sets used in the Lynden-Bell technique. For each data point with (L_i, z_i), the solid line represents the minimum luminosity or maximum redshift that the burst could have had and still have been observed. Employing the Lynden-Bell technique with associated sets defined as $N_j\,[L_j < L < \infty, 0 < z < z_{\max}(L_i)]$ produces the cumulative distribution for the vertical axis, whereas the M_j associated set produces the distribution for the data represented on the horizontal axis.

The modified version of this rank statistic proposed by Efron & Petrosian (1992) to test the independence of truncated data is based on a simple concept. Instead of measuring the ranks R_i for the entire set of observables, deal with data subsets that can be constructed to be independent of the truncation limit suffered by the entire sample. This is done by creating "associated sets," which include all objects that could have been observed given a certain limiting luminosity. We can define an associated set as

$$J_i \equiv \{\, j : L_j > L_i,\ L_{\lim,\,j} < L_i \}. \tag{6}$$

In other words, for each burst i there can be constructed a data subset that includes all events within the range $L_i < L < \infty$ and $0 < z < z_{\max}(L_i)$. The boundaries of an associated set for a given burst i are shown as dotted lines in Figure 3. In this scenario, we expect the rank R_i of z_i within the associated set

$$R_i \equiv \{\, j \in J_i : z_j \leq z_i \} \tag{7}$$

to be uniformly distributed between 1 and N_j, where N_j is the number of points in the associated set J_i. Using these new ranks, we can again construct the mean and variance, except that now we replace N with N_j such that $E = (1/2)(N_j + 1)$ and $V = (1/12)(N_j^2 - 1)$. The specialized version of Kendell's τ statistic is now given by

$$\tau = \frac{\Sigma_i (R_i - E_i)}{\sqrt{\Sigma_i V_i}}, \tag{8}$$

where the mean and variance are calculated separately for each associated set and summed accordingly to produce a single value for τ. This parameter represents the degree of correlation for the entire sample with proper accounting for the data truncation. With this statistic in place, it is a simple matter to find the parameterization that best describes the luminosity evolution. This is accomplished by first choosing a functional form for the luminosity

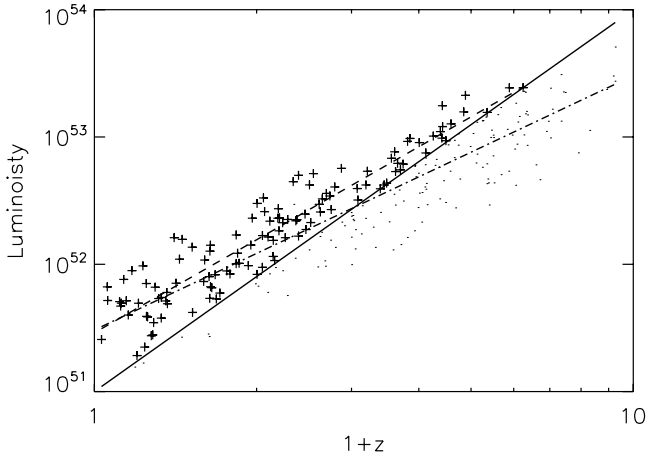

FIG. 4.—Generated luminosity and redshift data used to test the ability of the Efron & Petrosian method to estimate the correlation strength and functional dependence for data of a given flux cut. [*See the electronic edition of the Journal for a color version of this figure.*]

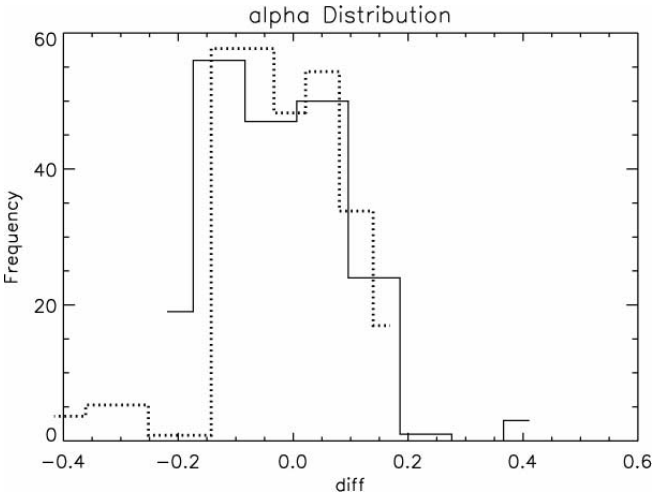

FIG. 5.—Histogram of the difference between the known correlation index and the reconstructed index ($p - q$) for a large set of generated (L, z) data with arbitrarily imposed flux thresholds. The error in the method is tightly centered around $p - q = 0$.

evolution, which in our case means choosing a simple power-law dependence $g(z) = (1 + z)^{\alpha}$. We can then make the transformation $L \rightarrow L' = L/g(z)$ and vary α until $\tau \rightarrow 0$.

An example of how well these methods are able to estimate underlying correlations in truncated data is shown in Figure 4. Here we have plotted a distribution of fake luminosity and redshift data with some known power-law dependence $L \propto (1 + z)^p$, which is subjected to a flux cut $L_{\rm lim} \propto (1 + z)^q$, represented by the solid line. The crosses show the observable data, whereas the dots represent the data that would otherwise be undetectable. The long-dashed line is the best fit to the truncated data without any knowledge of the flux cut, whereas the dash-dotted line is the reconstructed correlation when taking into account the flux threshold. This method fails when the undetected data points become significantly larger than the observable data set, with the exact boundary at which this occurs depending on the difference in the power-law indices between the underlying correlation and the flux threshold. Since these quantities cannot be known a priori, it is explicitly assumed that a large data sample contains a sufficient number of events above the flux threshold for the method to work. A histogram of the difference between the known correlation index and the reconstructed index ($p - q$) for multiple such simulations is shown in Figure 5. The error, or difference between the known p and the measured q, is peaked about zero with an FWHM that roughly matches the error estimates that correspond to the 1 σ range for this parameter given by the condition $|\tau| < 1$.

3.2. *Determination of Distribution Functions*

Once a parametric form that removes the correlation between L and z is known, it is possible to use nonparametric maximum likelihood techniques to estimate the underlying parent luminosity and redshift distributions. This luminosity distribution $\Phi(L_i)$ represents the cumulative GRB luminosity function, with the redshift distribution $\sigma(z_i)$ representing the GRB density evolution. Petrosian (1992) has shown that many, if not most, of the familiar nonparametric methods used in astronomy to produce $\Phi(L_i)$ and $\sigma(z_i)$ reduce fundamentally to Lynden-Bell's C method. Consider the area, or number of events, in the box produced by the associated set shown in Figure 3. If N_1 represents the number of points with $L \geq L_1$, then let dN_1 represent the number of points in the infinitesimal column between L_1 and $L_1 + dL_1$. The general premise behind the C method is that if the two variables (L, z) are stochastically independent, then the ratio between N_1 and dN_1 should equal the ratio between $d\Phi$ and the true cumulative distribution function $\Phi(L_1)$

$$\frac{dN_1}{N_1} = \frac{d\Phi}{\Phi_1}, \tag{9}$$

which can then be integrated to find $\Phi(L)$. In the case of discrete data points, this integration becomes a summation, yielding the solution

$$\Phi(L_i) = \prod_{k=2}^{j} \left(1 + \frac{1}{N_j}\right), \tag{10}$$

where N_j, is the number of bursts in the box defined by $0 < z < z_{\rm max}(L_j)$ and $L_j < L < \infty$. The value N_j is the same as Lynden-Bell's C_j^- in that it does not count the L_i object that is used to form the associated set. Similarly, we can construct the underlying cumulative redshift distribution function $\sigma(z_i)$ by reversing the definition of the associated set such that M_j represents the number of bursts in the box $0 < z < z_i$ and $L_{\rm min}(z_i) < L < \infty$. Then

$$\sigma(z_i) = \prod_{k=2}^{j} \left(1 + \frac{1}{M_j}\right). \tag{11}$$

As mentioned in § 1, there are several important limitations to the C method. First, the overall normalization of $\Phi(L_i)$ and $\sigma(z_i)$ is arbitrary, so information regarding the absolute numbers and densities cannot be obtained. Despite this, the shape of the bivariate distribution is constructed in such a way that it accounts for the data truncations. Due to this limitation, all distributions presented in this paper have arbitrary normalizations. Second, it is clear from equations (10) and (11) that the cumulative distribution function is not defined when either N_j or M_j is zero. This limitation restricts the use of the C method to samples with

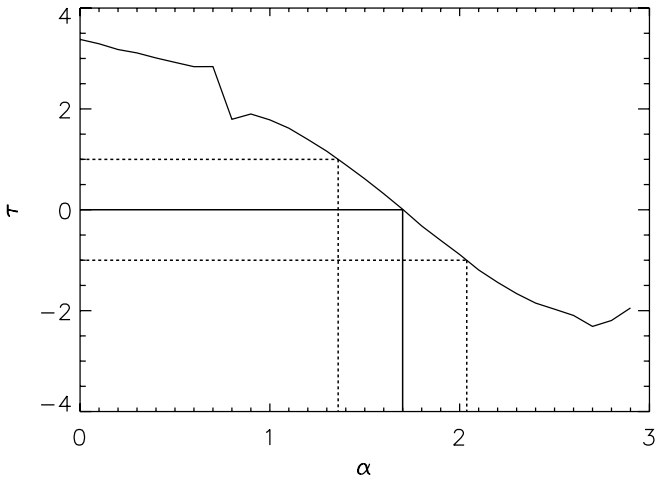

FIG. 6.—Correlation statistic τ plotted as a function of power-law index $g_\alpha(z) = (1+z)^\alpha$ parameterizing the luminosity evolution. The solid line represents the α index that minimizes the correlation between L' and z. The dotted lines show the 1 σ *statistical* error in the α-parameter.

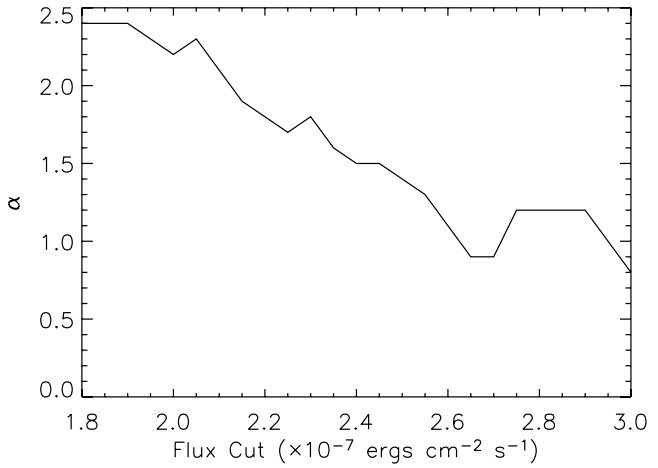

FIG. 7.—Correlation parameter α plotted as a function of the flux cut applied to the BNB04 sample. The optimal α is highly dependent on the choice of the cut value, showing the importance of a good understanding of the detector flux threshold.

a data size sufficiently large to ensure that all associated sets greater than $j = 2$ contain a nonzero number of points.

4. RESULTS

4.1. *Luminosity Evolution*

We apply the test of independence outlines in § 3.1 to the entire BNB04 GRB sample to test for luminosity evolution. For this analysis we use the flux threshold suggested by BNB04 of $f_{\min} = 0.5$ photons cm^{-2} s^{-1}, decreasing the sample size to 985 bursts. Applying this method, we find evidence for a strong 11.63 σ correlation between luminosity and redshift. This evolution is well parameterized by a power law of the form $g(z) = (1+z)^\alpha$, with an optimal value for the power-law index [i.e., when $\tau(\alpha) = 0$, given the transformation $L \rightarrow L' = L/g(z)$] of $\alpha = 1.7 \pm 0.3$. The error estimates on α correspond to the 1 σ range for this parameter given by the condition $|\tau| < 1$. A plot of $\tau(\alpha)$ versus α with the corresponding 1 σ levels is shown in Figure 6. These findings indicate that the average luminosity (modulo a beaming factor $d\Omega$) of GRBs in the universe has evolved with time. Because of the lack of beaming information, it may also be possible that the luminosity is remaining constant while the beaming factor $d\Omega$ is actually evolving. As is discussed in § 5, there is no observational evidence to suggest that this is the case.

It should also be noted that $\tau(\alpha)$ appears to be strongly affected by the choice of the flux threshold assumed for the sample. Plotted in Figure 7 is the optimal value for α versus $f_{\min}$. Not surprisingly, if we assume no flux threshold (i.e., $f_{\min} = 0$), τ approaches the overestimated value received from the standard Kendell τ statistic. Similarly, α approached the value obtained by simply performing a power-law fit to the truncated data. In this case α decreases steeply with increasing $f_{\min}$, never reaching a stable plateau, as one would hope would happen - as the $f_{\min}$ approaches the *true* threshold of the detector. This underscores the importance of having a good understanding the thresholds of the detector used to collect the sample. BNB04 make a strong case for a threshold of $f_{\min} = 0.5$ photons cm^{-2} s^{-1}, based on where they see a strong dropoff of detected events in the *L*-*Z* plane (see their Fig. 4), and we adopt this value for all analysis presented in this paper.

4.2. *Luminosity Function*

The deduced parametric form describing the luminosity evolution allows us to use the *C* method on the uncorrelated parameters L' and Z to obtain the cumulative luminosity function $\Phi(L')$. Shown in Figure 8 is the cumulative $\Phi(L')$ distribution plotted as $\Phi(>L')$ as a function of L' for all 985 bursts. Because the luminosity evolution has been explicitly removed, this distribution represents the luminosity function in the present epoch. Fitting a double power law to the curve yields $\Phi(>L') \propto L'^{-0.623}$ and $\Phi(>L') \propto L'^{-1.966}$ for the low- and high-luminosity ranges, respectively, separated by a break at a luminosity of roughly $\sim 10^{52}$. These slopes are very similar to those reported by Lloyd-Ronning et al. (2002), who found a GRB cumulative luminosity function with power-law slopes of $k_1 = -0.51$ and $k_2 = -2.33$ below and above a break at about $L' = 5.9 \times 10^{51}$. These values can also be compared to the luminosity functions found by Maloney & Petrosian (1999), who use the *C* method to account for selection effects in quasar samples. They find that the quasar luminosity function exhibits a double power-law form, with indices of $k_1 = -1.16$ and $k_2 = -3.59$.

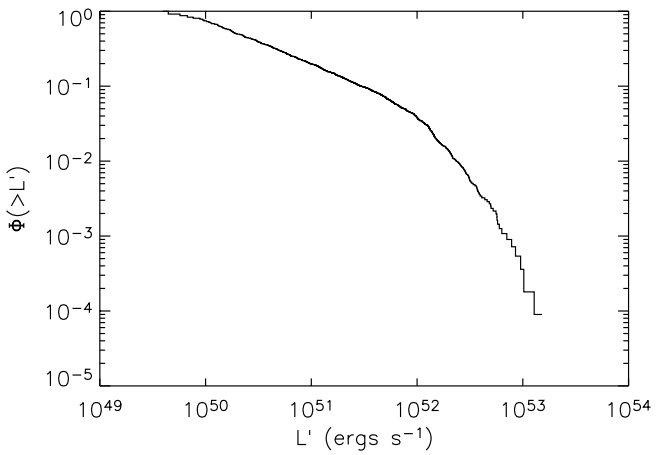

FIG. 8.—Cumulative luminosity function $\Phi(>L') = \int_{L_0}^{\infty} \psi(L')\, dL'$ representing the total number of events with L' or greater. The vertical normalization is arbitrary, but the method used to create $\Phi(L')$ successfully accounts for selection effects imposed by detection thresholds

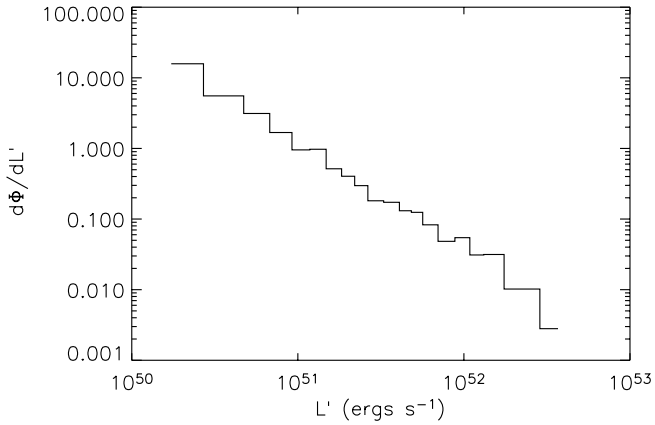

FIG. 9.—Present-epoch GRB luminosity function $\psi(L') = d\Phi/dL'$, representing the number of events between the luminosity L' and $L' + dL'$. The function falls as roughly $\propto L'^{-1.5}$ for luminosities below the break energy of 10^{52} ergs s^{-1}.

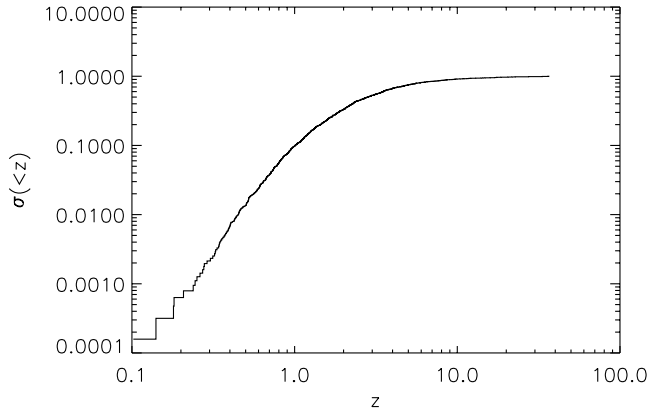

FIG. 10.—Cumulative density distribution $\sigma(z) = \int_0^z \rho(z)(dV/dz)\,dz$, representing the total number of events up to a given redshift. The flattening at high redshift indicates a dropoff of events around $z \sim 5$–10.

Next, we differentiate the cumulative luminosity function with a three-point Lagrangian interpolation to find the differential luminosity function $d\Phi/dL'$, or what is commonly referred to as simply the luminosity function $\psi(L')$. This function represents the total number of bursts with luminosity between L' and $L' + dL'$. A plot of $\psi(L')$ versus L' is shown in Figure 9. The function falls roughly as $\psi(L') \propto L'^{-1.5}$ below the break energy of $\sim 10^{52}$, with a sharp decline for higher L'. This power-law index is identical to the slope ($L'^{-1.5}$) found by Lloyd-Ronning et al. (2002) and similar to the index found by Schaefer et al. (2001), who found $L^{-1.7\pm0.1}$ from (L, z) data estimated from a combined use of the lag-luminosity function and variability-luminosity function, although the latter did not account for any selection biases in their data set. This value is also similar to results of several studies that used the measured flux distribution with an assumed density distribution $\rho(z)$, such as (Schmidt 2001), who uses the SFR to infer a $\rho(z)$ and finds $\psi(L') \propto L^{-1.4}$. The shape of the GRB luminosity function has important implications for jet model theories that predict specific power-law indices for various jet structures. A comparison between theorized shapes and our deduced values is discussed in more detail in § 5.

4.3. *Density Evolution*

Using the alternative definition of the associated set, we can construct the cumulative density distribution $\sigma(z) = \int_0^z \rho(z)(dV/dz)\,dz$, or the total number of GRBs per comoving volume, up to a given redshift. The cumulative distribution is shown in Figure 10 plotted as $\sigma(>z)$ as a function of z. The distribution of GRBs appears to increase smoothly with z, without a pronounced break at any distance, but with a flattening at high redshift indicating a dropoff of events between $5 \leq z \leq 10$. To get a better look at this density evolution, we can plot the cumulative density distribution $\sigma(z)$ as a function of comoving volume $V(z)$ as seen in Figure 11. If the density of GRBs per comoving volume $V(z)$ is constant, i.e., $\rho(z) = \rho_0$, then it should follow that $\sigma(z) \propto V(z)$. We can test for evolution by fitting $\sigma(z)$ versus $V(z)$ to a simple power law $\sigma(z) \propto V(z)^{\beta}$ and looking for deviations from the constant density case. An index of $\beta \neq 1$ indicates the presence of density evolution, with $\beta > 1$ and $\beta < 1$ signifying an increasing and decreasing population, respectively. Using the definition of $V(z)$ in a flat universe of

$$V(z) = \frac{4\pi}{3}\left[\frac{c}{H_0}\int_0^z \frac{dz}{\sqrt{\Omega_m(1+z)^3 + \Omega_\Lambda}}\right]^3, \qquad (12)$$

we find that the cumulative density distribution increases with z roughly as $\sigma(z) \propto V^{1.25}$ at low redshifts before falling off at higher redshifts. From these results we can deduce that the GRB density has undergone complicated evolution, increasing as $\rho \sim V^{0.25}$ before peaking between $z \sim 1$–2 and then decreasing. To obtain a more quantitative look at the shape of the comoving rate density $\rho(z)$, we again use a three-point Lagrangian interpolation routine on $\sigma(z)$ to find the differential cumulative distribution $d\sigma/dZ$. We can then convert this differential distribution into a comoving rate density through the relation:

$$\rho(Z) = \frac{d\sigma}{dZ}(1+z)\left(\frac{dV}{dZ}\right)^{-1}. \qquad (13)$$

In Figure 12 we show the resulting comoving rate density plotted as a function of z. It can be seen that the GRBs density function increases out to a redshift between $1 \leq z \leq$ and then flattens before beginning to show signs of a turnover at a redshift of $z > 3$. This is in contrast to previous estimates of the comoving rate density by Schaefer et al. (2001), Lloyd-Ronning et al. (2002), and Yonetoku et al. (2004), all of whom find a flattening of the GRB population with no apparent turnover out to a redshift of $z \sim 10$. It is also in contrast to results reported by Murakami et al. (2003), who also used the lag-luminosity correlation to estimate

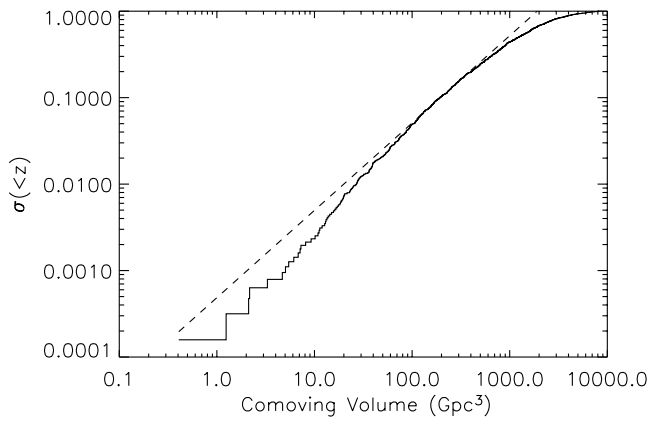

FIG. 11.—Cumulative density function $\sigma(z)$ plotted as a function of comoving volume. The dashed line represents the increase in the number of sources if the GRB density were constant throughout the history of the universe. The GRB density has increased as $\rho \sim V^{0.25}$ before peaking between $z \sim 1$–2 and then decreasing.

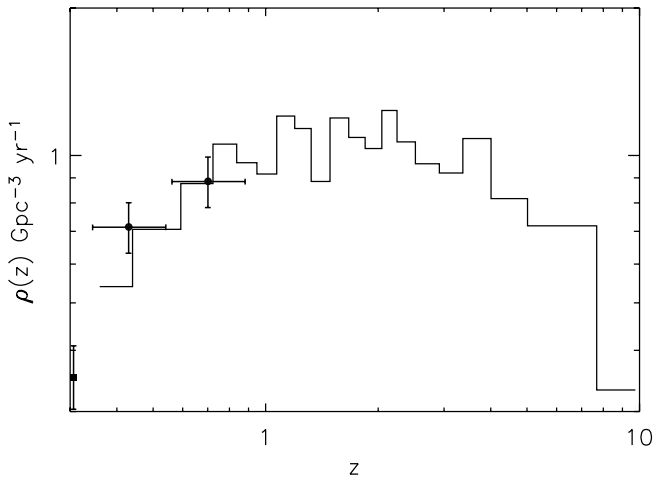

FIG. 12.—Comoving rate density $\rho(z)$ as a function of redshift. The rate density of sources can be seen to follow the evolution deduced from Fig. 11, increasing to a redshift of 1–2 then flattening before decreasing at higher redshifts. The circles represent high-redshift CC rates from Dahlen et al. (2004), whereas the square point is the local rate found Cappellaro et al. (1999). The increase in the CC event rate with redshift qualitatively matches the overall increase in the GRB comoving rate density.

the GRB formation rate. There the authors find the GRB formation rate increases steadily out to a redshift of at least 4, but it should be noted that this work did not take into account the detector selection effects discussed above, so a direct comparison may not be appropriate. As opposed to these previous findings, the turnover observed in our data quantitatively matches the global behavior of the SFR of the universe, which has been observed to peak between $1 \leq z \leq 2$ followed by a steady decline (Madau et al. 1996; Steidel et al. 1999). A more detailed comparison between the GRB comoving rate density and the supernova and star formations rates will be continued in § 5.

5. DISCUSSION

We find an 11.63 σ correlation between the luminosity and redshift data deduced from the lag-luminosity correlation, strongly suggesting an evolution of the average luminosities of GRBs. We show that this correlation can be parameterized as a power law as $L(z) = (1+z)^{1.7\pm0.3}$. This value agrees extremely well with the results presented in Lloyd-Ronning et al. (2002), who found a power-law index of $\alpha = 1.4$ after performing a similar analysis on (L, z) data estimated using the variability-luminosity correlation. These results imply that the average energy emitted per unit time per unit solid angle by GRBs was much higher in the distant past compared to relatively recent events. This is consistent with previous studies showing strong source evolution and also recent observations of underluminous nearby GRBs. Due to our lack of knowledge regarding the beaming angle of the bursts in our sample, it is also possible that the increase in the apparent luminosity is due to an increasing collimation at higher redshifts. As we discuss in more detail below, we find no evidence for beaming angle evolution in the current sample of GRBs with known redshift and jet opening angle, suggesting that this increase in luminosity cannot be due simply to an evolution of the collimation of the gamma-ray emission.

5.1. *Comparison to Other Objects*

Such a steep luminosity evolution is not uncommon in other astrophysical objects that show evolution with redshift. Maloney & Petrosian (1999) perform a similar analysis using the statistical techniques described in this paper on a combination of several quasar samples and find that the quasar luminosity function evolves as $L(z) = (1+z)^{2.58}$ up to a redshift of at least 2. There is evidence that this evolution may then become constant up to a redshift of at least 3 (Boyle et al. 1993). We find no such break in the luminosity evolution of GRBs, which in our case can be adequately fit by a single power law between at least $0 < z < 10$. The authors also find a density evolution of $\sigma(z) \propto V^{1.19}$ similar to the power law of $\sigma(z) \propto V^{1.25}$ that we find in GRBs at low redshifts. A more detailed look at their comoving rate density estimate shows that the quasar density rises as $\rho \sim (1+z)^{2.5}$ before peaking at $z \approx 2$ and then declining rapidly, as roughly $\rho(z)\ (1+z)^{-5}$ for $z > 2.0$. This is qualitatively similar to the trend we deduce from the GRB sample, which rises as $\rho \sim (1+z)^{2.4}$ to $z \approx 1$, although the preceding decline is much more shallow, as $\rho \sim (1+z)^{-0.6}$, and extends to at least a redshift of $z \approx 6$ before dropping off sharply.

There is also evidence for significant evolution in the luminosities of star-forming galaxies, which is perhaps a more relevant comparison to GRBs because of their suggested association with active star-forming regions (Djorgovski et al. 1998). Hopkins (2004) used a compilation of recent SFR density measurements as a function of redshift to constrain the evolving luminosity function of star-forming galaxies. He finds that the preferred evolution in a standard cosmology is given by $L(z) = (1+z)^{2.70\pm0.60}$ out to a redshift as high as $z \approx 6$. At the same time he finds evidence for a very shallow density evolution given by $\rho(z) \sim (1+z)^{0.15\pm0.60}$, markedly different from steep density evolution $\rho(z) \sim (1+z)^{2.5}$ that we estimate for GRBs at low redshift. This would indicate that GRB luminosities have evolved at a slower rate but that their density in the past rises much more steeply compared to the number of star-forming galaxies. It could also mean that the number of GRBs per star-forming galaxy has evolved rapidly with cosmic time.

Perhaps more interesting is the comparison of the GRB comoving rate and luminosity densities with the global SFR history of the universe. Because GRBs suffer little extinction and are potentially detectable out to redshifts of $z \approx 10$, they could offer a unique tracer to the SFR history. They would allow for a more complete sampling of dust enshrouded star-forming regions that may be missed in traditional SFR estimates based on the UV "dropout" technique that is currently employed to identify Lyman break galaxies. The shape of the SFR at low redshifts $z < 1$ is relatively well understood, showing an order of magnitude increase from $0 \leq z \leq 1$ (Madau et al. 1996; Fall et al. 1996). These early estimates suggest that star formation activity peaks around $z \sim 1$, followed by a rapid decline at higher redshifts. However, further observations of hundreds of Lyman break galaxies at redshifts of $z \sim 3$ and 4 have shown that the SFR may remain constant after reaching a maximum around $1 \leq z \leq 2$ (Steidel et al. 1999). Recent deep surveys with the Subaru Telescope (Iwata et al. 2003) and the *Hubble Space Telescope* (*HST*; Bouwens et al. 2003) out to $z \sim 5$ and 6 show evidence for a mild evolution of the SFR at redshifts $z > 3$, with measurements based on photometric redshifts showing a constant SFR out to $z \approx 6$ (Fontana et al. 2003). These recent SFR estimates qualitatively match the deduced GRB comoving rate density shown in Figure 12. At low redshifts ($z < 1$), the GRB rate density increases as $\rho(z) \sim (1+z)^{2.5}$, roughly matching the rise in the SFR over the same range, with a peak somewhere between $1 \leq z \leq 2$. The following flattening and decline between $2 \leq z \leq 6$ in the GRB $\rho(z)$ matches the global properties of the SFR estimated from the recent deep surveys.

Of course, the comparisons between the GRB comoving rate density and the SFR are simply phenomenological, since we

have as of yet no way of connecting the amount of star formation for a given number of GRBs. Ultimately, this conversion factor depends on knowledge of the GRB progenitor and the stellar initial mass function (IMF) and how it changes with redshift. In the case of the collapsar model (Woosley 2000; MacFadyen & Woosley 1999), the rate of GRBs produced for a given SFR would increase sharply with redshift, as is the case for all core collapse events, due primarily to redshift dependence on the IMF. However, the connection between the GRB $\rho(z)$ and the SFR would be straightforward, since the progenitors would consist of massive stars with short lifetimes, making them direct indicators of the SFR at that redshift. If the mass range of the progenitors and the redshift dependence of the IMF is known (or assumed) then it would be possible to calculate a constant that directly relates $\rho(z)$ to the SFR. The case is more complicated for binary merger models, since there would be a substantial delay between the formation of the progenitor star and the final merger event that produces the GRB. The distribution in the delay times is not well known for SNe events, much less GRBs, but it is expected to be large enough to dissociate the GRB $\rho(z)$ and the active SFR at a given redshift. The peak we observed in our deduced values for $\rho(z)$ matching the peak of the current SFR estimates hardly seems coincidental, tentatively favoring the core collapse models.

It is interesting then to compare our demographic results to that of various types of supernovae. There is overwhelming observational evidence and theoretical discussion suggesting a GRB-SN connection, including observations of supernova bumps in afterglow light curves (Stanek et al. 2003; Hjorth et al. 2003) and a deduced collimation-corrected energy that is narrowly clustered around the typical SN energy of 10^{51} ergs (Frail et al. 2001; Bloom 2003). Although the intrinsic luminosity of type Ia SNe are *a priori assumed* to be constant with redshift (hence no luminosity evolution), we can still compare the formation rates of SNe Ia/b/c to GRBs, although the b/c events are obviously of more relevance to GRB models. Unfortunately, very little SNe data are available for the high-z universe, with only seven SNe at $z > 1.25$ of the 42 SNe detected in the redshift range of $0.2 \leq z \leq 1.6$ by the Advanced Camera for Surveys (ACS) on *HST* (Riess et al. 2004). Data on core collapse supernovae account for only 17 events in this sample, going out to a maximum range of $z \approx 0.7$. Dahlen et al. (2004) use these data to estimate the core collapse SNe (CC SNe) rate between $0.3 \leq z \leq 0.7$ and find a steep (about a factor of $\sim$7) increase in the SNe $\rho(z \approx 0.7)$ compared to the local rate presented by Cappellaro et al. (1999). Shown in Figure 12 are their data points for CC SNe plotted over the GRB comoving density, both rates normalized to 1 at $z = 0.7$. The two data points, although limited, do agree with the rise of the GRB $\rho(z)$. A direct SNe-GRB comparison at higher redshifts will have to wait until the launch of the *SNAP* spacecraft, which is predicted to find thousands of supernovae, including a significant number at high redshift.

5.2. *The Nature of the Luminosity Evolution*

The luminosity evolution that we observed in the (L, z) data leads to the conclusion that the GRB progenitor population has most likely evolved in such a way as to create more energetic or more narrowly beamed bursts in the distant past. Speculations on the nature of this evolution depend on the progenitor model and on how the properties of their population are affected by the conditions of the early universe. In the case of highly rotating massive stars (i.e., the collapsar model), the overall progenitor mass and/or rotation rate could be the determining factor. There is ample evidence suggesting that the so-called Population III stars were much more massive than their present day counterparts. This is suggested by recent work showing that the IMF has evolved with time, having a much higher value in the distant past. This higher IMF is due to various factors, although it primarily is due to the lower metallicity in the early universe. The amount of material lost to stellar ejecta has also been shown to depend on stellar metallicity, causing these early stars to retain more of their mass until their eventual collapse.

Although the relationship between progenitor mass and emitted energy and/or beaming angle is not straightforward, there are reasons to think that this increase in average mass could result in an increase in the total energy budget available to a burst. MacFadyen & Woosley (1999) show that under the right conditions, the collapsar model could produce more energetic bursts with increasing stellar mass, up to some limit dictated by the energy needed by the GRB jet to punch through the stellar envelope. Proponents of black hole accretion disk models have also shown that the rate of accretion onto the central engine of the GRB increases dramatically as a function of the progenitor mass, increasing the overall energy available to the burst.

Unfortunately, a simple increase in the overall energy budget cannot by itself explain the deduced luminosity evolution. Frail et al. (2001) and Bloom et al. (2003) have recently shown observational evidence suggesting that the collimation-corrected GRB energies E_γ are actually narrowly clustered around the 10^{51} ergs typical of SNe explosions. They come to this conclusion by correcting the observed prompt isotropic equivalent energy release $E_{\rm iso}$ of several GRBs with known redshift by a factor of $1 - \cos\theta_j$, where θ_j is the canonical jet opening angle. These angles are derived from broadband breaks observed in the afterglow light curves attributed to the slowing of the GRB jet to the point at which the relativistic beaming angle of the radiation $1/\Gamma$ becomes greater than θ_j. Bloom et al. (2003), using a larger sample of bursts, show that the corrected energies cluster around 1.33×10^{51} ergs, with a variance of 0.35 dex, or a factor of 2.2. Guetta et al. (2005) have reported a similar result when correcting for the isotropic luminosity $L_{\rm iso}$, although theirs is not as narrow as the E_γ results. If the collimation-corrected energy and luminosity are indeed invariant with redshift, this directly implies that the brightening of the apparent isotropic equivalent luminosity is actually due largely to an increase in the beaming factor as a function of redshift and not an increase in the overall energy of the burst. There are physical arguments that can be made in the case of the collapsar model that would suggest that more massive progenitor stars could indeed produce more collimated jet outflows.

Plotted in Figure 13 are the E_γ estimates from Friedman & Bloom (2005) for a little more than two dozen GRBs. Furthermore, plotted in Figure 14 is the canonical jet opening angle for the same two dozen GRBs. By apply a standard Kendall rank order τ statistic we can measure the degree of correlation in these two samples in a nonparametric way (i.e., without assuming an underlying correlation type). We find a correlation strength of $\tau = 0.093$ between E_γ and redshift and $\tau = 0.163606$ between θ_j and redshift, where a τ of 1 signifies a significant correlation. Therefore, there is no deduced redshift dependency that would suggest any evolution of the jet opening angle or E_γ with redshift in the pre-*Swift* data set. This lack of redshift dependency stands to be tested in the *Swift* era as more GRBs with measured jet break times are observed over a broader redshift range. Nevertheless, if it is confirmed it would imply that the evolution of some jet property other than the collimation factor must be responsible for the brightening of GRBs with redshift. Speculations on the nature of this evolution depend on the jet model used to explain

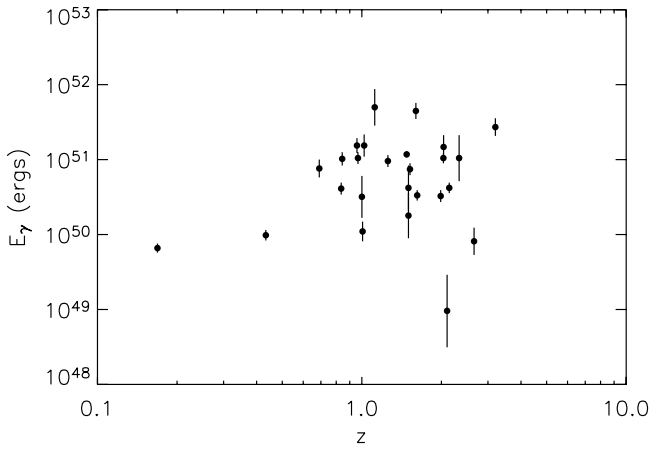

FIG. 13.—Plot of the collimation-corrected total emitted energy of 23 GRBs with known redshift and beaming angles. No significant correlation can be seen with redshift.

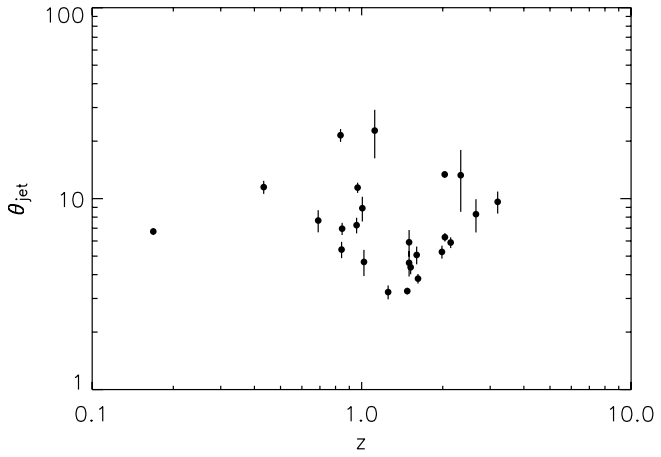

FIG. 14.—Beaming angles θ_j of 23 GRBs with known redshift. The lack of a significant correlation with redshift is quite evident.

the emission. The simplest model assumes a uniform energy distribution per solid angle $\epsilon(\theta)$ across the jet, with a sharp drop beyond θ_j. In this scenario, the observed distribution in GRB energies is directly due to the diversity of jet opening angles, as are the observed values of the jet break time t_j. The lack of any concrete evidence for an evolution of θ_j with redshift, combined with the observation that the collimation-corrected E_γ and L_γ are very narrowly clustered, creates difficulty for the uniform jet model to explain any kind of evolution in luminosity. One of the observed conditions noted above would have to be broken in order to accommodate any such evolution with this model.

In a structured jet model, the GRB jets are identical, having a quasi-universal shape with a fixed opening angle and a non-uniform energy distribution per solid angle. The diversity in the observed jet break time and isotropic energies would then be a result of varying viewing angles away from the jet axis θ_v. Furthermore, an observer viewing the GRB at a small θ_v would see an extremely powerful burst, with the observed luminosity declining as some function of increasing θ_v. A jet structure with a functional form of $\epsilon(\theta)^{-2}$ is required to reproduce the observed $t_j \propto E_{\rm iso}$, i.e., the Frail et al. (2001) and Bloom et al. (2003) results. If the requirement of a narrow E_γ and L_γ distribution is broken, then any power-law structure θ^k could still produce the observed steepening in the afterglow light curve. In this case, the luminosity evolution would manifest itself not as a narrowing of θ_j, but rather as an overall increase in the normalization of $\epsilon(\theta_j)$. Another possibility would be an evolution of the morphology of $\epsilon(\theta)$ as a function of redshift. If the power-law index $\epsilon(\theta_j) \sim \theta_j$ has evolved with time, or if $\epsilon(\theta_j)$ has evolved from a non-power-law shape (e.g., a Gaussian profile), such that $\epsilon(\theta_j)$ varies more slowly with viewing angle, then there would be a markedly different luminosity distribution at high redshift. A third, rather implausible, explanation is a preferentially small viewing angle θ_v at higher redshift, although there is no physical reason to think that this is at all possible. Therefore, it would seem that evidence of luminosity evolution in the presence of the observation that E_γ and L_γ are narrowly distributed and the lack of any evidence of an evolution of θ_j with redshift, favors a quasi-universal jet model over a uniform jet model. This is primarily due to the inability of the uniform jet model to explain any kind of luminosity evolution with redshift without a parallel evolution in the jet opening angle, something that is not currently observed.

5.3. *Luminosity Functions and Jet Model Discrimination*

Because the energy distribution $\eta(\theta_j)$ of the structured jet model is well defined, it can make specific predictions regarding the GRB luminosity function $\phi(L)$. In the case of power-law-structured jets $\epsilon(\theta_j) \propto \theta_j^{-k}$, resulting in a predicted luminosity function with a slope of $\gamma = 1 + 2/k$ (Zhang & Mészáros 2002). The "canonical" $k = 2$ model would yield a luminosity function $\propto L^{-2}$ (Rossi et al. 2002), whereas the quasi-universal Gaussian-structured jet model predicts $\propto L^{-1}$ (Lloyd-Ronning et al. 2004). Although the uniform jet model also exhibits a well-defined $\epsilon(\theta_j)$, it cannot make any firm predictions about the shape of the GRB luminosity function due to the random variation of θ_j.

The luminosity function deduced from our analysis is well fit by a single power law with an index of $\propto L'^{-1.5}$ for luminosities below about 10^{52}, with a sharp decline for higher luminosities. This value is intermediate between the expected value for the $k = 2$ power-law and Gaussian-structure models. An index of $L'^{-1.5}$ actually predicts a power-law model with $k = 4$, which is much steeper than the $k = 2$ shape needed to keep $E_{\rm iso}\theta^2$ roughly constant. It is also possible that a simple Gaussian or power-law profile for $\eta(\theta)$ is simply an oversimplification. It has been pointed out by Lamb & Graziani (2003) that $\eta(\theta)$ would have to fall off steeper than θ^{-2} at large angles if the quasi-uniform jet model is to explain the relative numbers of X-ray flashes to GRBs. This may explain why so many studies have found a sharp decline above some break energy, possibly indicating a different value for k at low and high luminosities, i.e., large and small opening angles, respectively. In any case, it is not impossible to think that the jet morphology is more complicated than a simple power-law or Gaussian profile, as is suggested by our results.

6. CONCLUSIONS

In this work we perform demographic studies on a large sample of luminosity and redshift data found through the use of the lag-luminosity correlation. By applying maximum likelihood techniques, we are able to obtain an estimate of the luminosity evolution, luminosity function, and density distributions in a way that accounts for detector selection effects. We find that there exists a strong (11.63 σ) correlation between luminosity and redshift that can be parameterized as $L(z) = (1 + z)^{2.58}$. The resulting cumulative $\Phi(L')$ and differential $d\Phi/dL'$ luminosity functions are well fit by double power laws separated by a break

energy of about 10^{52} ergs s^{-1}, with $d\Phi/dL'$ exhibiting a power-law shape of $L^{-1.5}$ below this luminosity. This value does not immediately discriminate against any proposed structured jet models, but it may indicate that a more complicated jet profile is need to explain the observed luminosity function of GRBs. The GRB comoving rate density is found to increase as $\rho_\gamma(z) \propto (1+z)^{2.5}$ to a redshift of $z \approx 1$, followed by flattening and eventual decline before $z > 6$. Although, the conversion between $\rho_\gamma(z)$ and an estimate of the SFR cannot be quantitatively made due to the uncertainty regarding the GRB progenitors and their initial stellar mass functions, it can be said that $\rho_\gamma(z)$ does qualitatively follow recent photometric estimates of the SFR, as would be expected from massive short-lived progenitors. We stress that these conclusions are based on the validity of the lag-luminosity correlation, which still stands in need of confirmation as new redshift data become available. A full confirmation, and most probably further calibration, of this distance indicator will have to wait for additional detections with the *Swift* spacecraft, which should have the collecting area necessary to obtain high signal-to-noise ratio energy-dependent light curves from which to measure statistically significant lags. Even with the slew of directly measured luminosity and redshift data expected to come from the *Swift* mission, empirical distance indicators may still play an important role in expanding the available GRB data set through the use of archival BATSE and *BeppoSAX* data for statistical studies such as the analysis performed in this work.

REFERENCES

Amati, L., et al. 2002, A&A, 390, 81
Band, D., Norris, J., & Bonnell, J. 2004, ApJ, 613, 484
Band, D., et al. 1993, BAAS, 182, 7409
Bloom, J. S. 2003, PASP, 115, 271
Bloom, J. S., Frail, D., & Kulkarni, S. 2003, ApJ, 594, 674
Bouwens, R. J., et. al. 2003, ApJ, 595, 589
Boyle, B. J., Griffiths, R. E., Shanks, T., Stewart, G. C., & Georgantopoulos, I. 1993, MNRAS, 260, 49
Cappellaro, E., Evans, R., & Turatto, M. 1999, A&A, 351, 459
Dahlen, T., et al. 2004, ApJ, 613, 189
Djorgovski, S., Kulkarni, S., Bloom, J., Goodrich, R., Frail, D., Piro, L., & Palazzi, E. 1998, ApJ, 508, L17
Efron, B., & Petrosian, V. 1992, ApJ, 399, 345
Fall, S., Charlot, S., & Pei, Y. 1996, ApJ, 464, L43
Fishman, G. J., et al. 1994, ApJS, 92, 229
Fontana, A., Poli, F., Menci, N., Nonino, M., Giallongo, E., Cristiani, S., & D'Odorico, S. 2003, ApJ, 587, 544
Frail, D. A., et al. 2001, ApJ, 562, L55
Friedman, A., & Bloom, J. 2005, ApJ, 627, 1
Ghirlanda, G., Ghisellini, G., & Lazzati, D. 2004, ApJ, 616, 331
Guetta, D., Piran, T., & Waxman, E. 2005, ApJ, 619, 412
Hjorth, J., et al. 2003, Nature, 423, 847
Hopkins, A. M. 2004, ApJ, 615, 209
Ioka, K., & Nakamura, T. 2001, ApJ, 554, L163
Iwata, I., et al. 2003, PASJ, 55, 415
Kobayashi, S., Ryde, F., & MacFadyen, A. 2002, ApJ, 577, 302
Kocevski, D., & Liang, E. P. 2003, ApJ, 594, 385
Kulkarni, S. R., et al. 1998, Nature, 393, 35
Lamb, D., & Graziani, C. 2003, BAAS, 202, 4501
Lloyd-Ronning, N., Dai, X., & Zhang, B. 2004, ApJ, 601, 371
Lloyd-Ronning, N., Fryer, C., & Ramirez-Ruiz, E. 2002, ApJ, 574, 554
Lynden-Bell, D. 1971, MNRAS, 155, 95
MacFadyen, A. I., & Woosley, S. E. 1999, ApJ, 524, 262
Madau, P., Ferguson, H. C., Dickinson, M. E., Giavalisco, M., Steidel, C. C., & Fruchter, A. 1996, MNRAS, 283, 1388
Maloney, A., & Petrosian, V. 1999, ApJ, 518, 32
Murakami, M., Nishihara, K., & Hanawa, T. 2003, PASJ, 55, L65
Norris, J. P. 2002, ApJ, 579, 386
Norris, J. P., Marani, G. F., & Bonnell, J. T. 2000, ApJ, 534, 248
Petrosian, V. 1992, in Statistical Challenges in Modern Astronomy, ed. E. D. Feigelson & G. J. Babu (New York: Springer), 173
Phillips, M. M., Lira, P., Suntzeff, N. B., Schommer, R. A., Hamuy, M., & Maza, J. 1999, AJ, 118, 1766
Riess, A. G., et al. 2004, ApJ, 607, 665
Rossi, E., Lazzati, D., & Rees, M. 2002, MNRAS, 332, 945
Salmonson, J. D. 2000, ApJ, 544, L115
———. 2001, BAAS, 198, 3809
Sazonov, S., Lutovinov, A., & Sunyaev, R. 2004, Nature, 430, 646
Schaefer, B., Deng, M., & Band, D. 2001, ApJ, 563, L123
Schmidt, M. 2001, ApJ, 552, 36
Soderberg, A. 2004, Nature, 430, 648
Stanek, K. Z., et al. 2003, ApJ, 591, L17
Steidel, C. C., Adelberger, K. L., Giavalisco, M., Dickinson, M., & Pettini, M. 1999, ApJ, 519, 1
Woosley, S. E. 2000, in AIP Conf. Proc. 526, Gamma-Ray Bursts, ed. R. M. Kippen, R. S. Mallozzi, & G. J. Fishman (Melville: AIP), 555
Yonetoku, D., et al. 2004, ApJ, 609, 935
Zhang, B., & Mészáros, P. 2002, ApJ, 571, 876